Intraband Quantum Dot Barrier Devices - Optimization of Energy Level Alignment

ECS Transactions, 102 (1) 45-51 (2021)
10.1149/10201.0045ecst ©The Electrochemical Society

Intraband Quantum Dot Barrier Devices - Optimization of Energy Level Alignment

Shihab Bin Hafiz[a], Mohammad Mostafa Al Mahfuz[a], and Dong-Kyun Ko[a]

[a] Department of Electrical and Computer Engineering, New Jersey Institute of Technology, Newark, New Jersey 07102, USA

Mid-infrared barrier detectors constructed from intraband colloidal quantum dots brings the advantage of greatly simplified device fabrication procedure with the potential for high temperature operation. Here, we report the fabrication and characterization of vertically-stacked Ag_2Se / PbS / Ag_2Se quantum dot barrier devices with improved infrared responsivity. Through optimizing the energy level alignment, 4.5 μm responsivity now reaches 84.1 mA/W which results in 570 % improvement in specific detectivity compared to the first generation quantum dot barrier devices.

Introduction

Intraband quantum dots (QDs) have recently become of great interest for mid- to long-wavelength infrared applications due to their ability to form uniform, large area thin-films using low-cost solution processing (1,2) and the potential for high temperature operation (3,4). In these degenerately-doped semiconductor QDs, optical transition take place between the first and the second quantum confined energy levels (intraband or intersubband transition) and the their sparse density of state leads to suppression of Auger recombination process that can potentially allow photodetectors to operate with reduced cooling requirements (5). While intraband QDs have such benefits they also come with a drawback: film composed of intraband QDs are highly conductive and pose a significant challenge in realizing functional optoelectronic devices. Hence, many device research to date were limited to lateral photoconductive devices in which the distance between two electrodes were in the range of tens of micrometers (6,7). On the other hand, vertically stacked devices could not be realized due to the extremely high dark current originating from the short distance (100 - 200nm) between the top and bottom electrodes. To overcome this challenge, our group has recently demonstrated a barrier device design utilizing Ag_2Se intraband QDs as a mid-wavelength infrared absorber and PbS QDs as a potential barrier (8). The fabrication of this device is identical to creating vertical Ag_2Se QD photoconductor via layer-by-layer deposition but with an inclusion of PbS QD layer in the middle of the stack that forms a charge transport barrier. An 800% increase in the dark conductivity was observed compared to the device without the barrier and a 70-fold improvement in mid-wavelength infrared responsivity was measured compared to the lateral photoconductive devices. This infrared responsivity improvement is primarily attributed to the increased carrier collection efficiency arising from orders-of-magnitude reduction in the distance that the photogenerated carriers have to travel to reach the electrode.

The present work builds on the first generation barrier device to further improve the photodetector performance through energy level alignment optimization. In the first generation barrier device, the electron barrier formed by PbS QD layer was sufficiently high to inhibit the dark current but the height was not optimized with respect to Ag_2Se QDs. The ideal alignment would be the one shown in Figure 1, where the first quantum confined conduction energy level ($1S_e$) of PbS QD coincides with the second quantum confined conduction energy level ($1P_e$) of Ag_2Se QD. This alignment will not only result in a smaller dark current but also increase the photocurrent as the transport barrier for photoexcited electrons are minimized. In QD-based system, energy level alignment can be readily achieved through adjusting the size-dependent quantum confinement via controlling the QD size. We demonstrate this optimization by increasing the size of Ag_2Se QD while keeping the PbS QD size constant thereby moving the $1P_e$ of Ag_2Se QDs closer to $1S_e$ of PbS QDs.

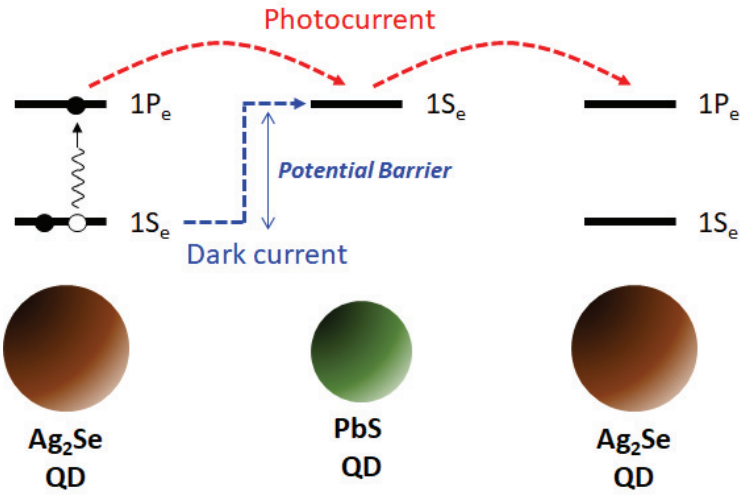

Figure 1. Schematic illustration of optimum energy level alignment between Ag_2Se and PbS QDs. $1S_e$ and $1P_e$ denote first conduction energy level and second conduction energy level of respective QDs.

Experiments

Ag_2Se and PbS QD Synthesis

Ag_2Se QDs with absorption peak centered at $\lambda = 4.7$ μm were synthesized by modifying the previously reported procedure (8). In a typical synthesis, 30 mL of oleylamine was degassed in a 250 mL three-neck flask for 1 hour under vacuum at 90 °C. 1 M TOP-Se and 0.5 M TOP-Ag precursor solutions were prepared inside the glovebox by dissolving Se powder and AgCl in trioctylphosphine (TOP), respectively. 8 mL of TOP-Se was injected to oleylamine under nitrogen atmosphere and the temperature of the mixture was increased to 130 °C. Then, 16 mL of TOP-Ag mixed with 800 μL diphenylphosphine (DPP), was rapidly injected to initiate reaction. The reaction was carried out for 30s and the color of the solution changed to dark brown. The synthesis was quenched by injecting 20 mL of butanol and cooled to room temperature in a water bath. The QDs were precipitated with a

mixture of ethanol and methanol. The final precipitate was redissolved in 5 mL of octane after three methanol washes.

The synthesis of PbS QDs with absorption peak at $\lambda = 1240$ nm was carried out following previously reported procedure (9). Lead oxide (0.45 g) was dissolved in 10 mL of 1-octadecene and 4 mL of oleic acid at 110 °C. The solution was degassed in a 50 mL three neck flask for 2 hours at vacuum. Then, 0.2 mL of hexamethyldisilathiane is added in 10 mL of 1-octadecene to prepare sulphur precursor solution, which was injected to initiate reaction at 150 °C under nitrogen atmosphere. The reaction temperature was maintained at 120 °C for 4 min and the solution was cooled down to room temperature with a water bath. The QDs were purified three times using ethanol and the final QDs were redispersed in a mixture of hexane/octane.

Optical Absorbance Characterization

A Thermo Nicolet 370 FTIR spectrometer was used to obtain optical absorption spectra of Ag_2Se QD films prepared on KBr card. Optical absorption spectra of PbS QDs dissolved in tetrachloroethylene were acquired using StellarNet UV-Vis-NIR spectrometer (RW-NIRX-SR and BLK-CXR).

Device Fabrication

QD-based barrier devices were fabricated on a glass substrate, where a bottom contact of 80nm (Cr/Ag) was deposited by thermal evaporation using a shadow mask. Ag_2Se and PbS QDs were deposited by spin coating at 2000 rpm for 30 s, where CQD films were ligand exchanged with 1,2-ethanedithiol (1,2-EDT). 10 layers of Ag_2Se QDs were first spin coated, then 4 - 5 layers of PbS QDs were deposited, followed by another 10 layers of Ag_2Se QDs. Then, Ag NW solution were spin coated at 2000 rpm for 30 s on top of QD film, which were used as infrared transparent contact. Finally, 120 nm top contact with two finger electrodes was deposited by thermal evaporation of Ag using a shadow mask.

Device Characterization and Photodetector Parameter Measurements

Current-voltage measurements were obtained by Agilent 4155 semiconductor parameter analyzer. A calibrated blackbody (900 °C) was used as an illumination source, where photocurrent was measured by lock-in technique utilizing a preamplifier (SR570) coupled with a lock-in amplifier (SR830). Spectral responsivity was measured with a set of Fabry-Perot band-pass filters, having center wavelengths varying from 2 to 7 μm. A spectrum analyzer (SR760) was used to measure the noise current density at 15 Hz, where SR570 preamplifier provided a low-noise bias to the device. All the instruments including the device were kept inside a Faraday cage and were grounded to avoid external noise.

Results and Discussion

Figure 2(a) shows the optical absorption of Ag_2Se QDs prepared via DPP-assisted synthesis (8). The intraband absorption peak is centered at 4.7 μm which corresponds to an average size of 6 nm. Other characteristic peaks around 3.4, 4.4, and 6.8 μm correspond to vibrational modes of C−H, CO_2, and trioctylphosphine (TOP), respectively. 5nm PbS QDs,

which will be used to form a barrier layer, were synthesized using previously reported procedure (9). The interband absorption peak of PbS QD is positioned at 1.24 μm, as shown in Figure 2(b). Based on the prior reports on the photoemission spectroscopy measurements on PbS (10) and Ag_2Se (11) QDs as well as the potential barrier height analysis conducted in our previous work (8), 6 nm Ag_2Se and 5 nm PbS QDs synthesized here form an ideal energy level alignment depicted in Figure 1.

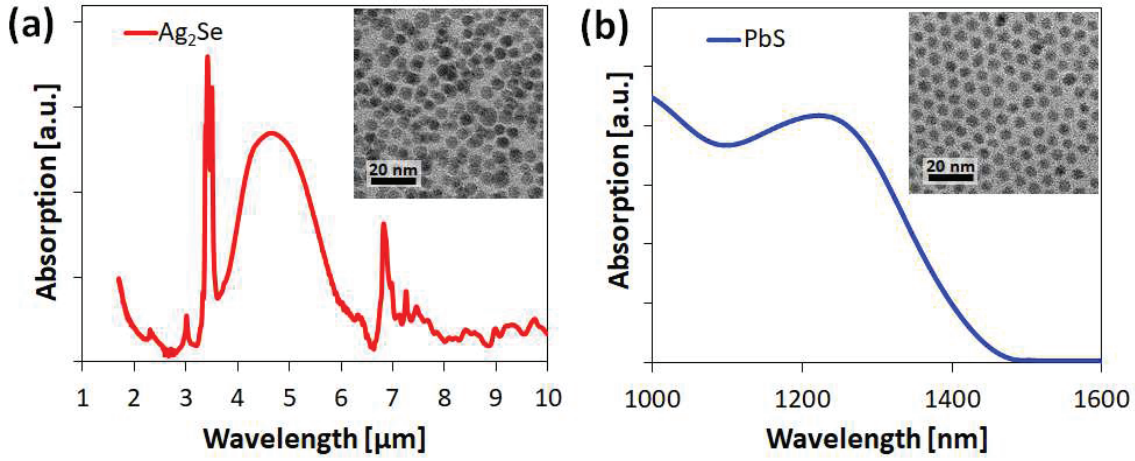

Figure 2. Optical absorption spectra of (a) Ag_2Se QDs obtained from Fourier transform infrared spectrometer and (b) PbS QDs obtained from near-infrared spectrophotometer. TEM images of QDs are shown as an inset.

Figure 3(a) shows a schematic illustration of our vertically-stacked barrier QD device. A glass substrate pre-patterned with Ag bottom electrode (using Cr as an adhesion layer), which forms an Ohmic contact with Ag_2Se QDs, were first prepared. Then Ag_2Se QD mid-infrared absorber layer were formed by repeating layer-by-layer QD deposition and ligand-exchange using 1,2-EDT. This was followed by PbS QD barrier layer deposition using the identical procedure used for Ag_2Se QD layer and completed with another thick layer of Ag_2Se QD. Ag nanowire mesh layer, which serves as infrared transparent conducting electrode, was formed via spin-casting. Lastly, current-collecting Ag finger electrodes was formed with a via-opening of 200 x 200 μm. This via-opening defines the device optical area (active pixel area).

Figure 3(b) shows the current-voltage (I-V) characteristics of the device obtained under dark. An I-V curve of a device constructed without the PbS QD barrier layer is also overlaid for comparison. Both I-V curves show linear Ohmic behavior. The uniqueness of our QD barrier device design arise from the fact that insertion of PbS QD barrier layer does not change the contact property since even for the barrier device, top and bottom Ag is in contact with the Ag_2Se QD layers. This greatly simplifies the device fabrication procedure and enables direct transition from rudimentary photoconductor devices to advanced heterojunction stack devices. From the slope of the I-V characteristics, device resistance values can be extracted. The barrier device shows 910 % increase in the resistance compared to the one without the PbS QD barrier. This is in agreement with Figure 1 where $1S_e$ of PbS QD act as a potential barrier for ground state electrons in $1S_e$ of Ag_2Se QD

which give rise to the dark current. Compared to the first generation of QD barrier devices (8), optimization of energy level alignment results in 14% improvement in the dark resistivity.

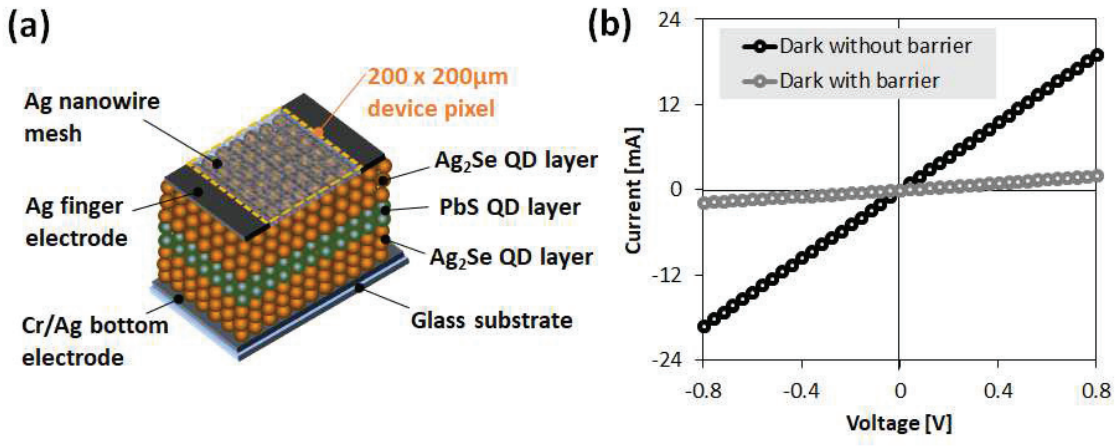

Figure 3. (a) Schematic illustration of the fabricated device structure. (b) Current-voltage characteristics under dark obtained from devices with and without PbS QD barrier layer.

While the improvement in the dark resistivity is small, we observe a large enhancement in the infrared response in the device with energy level alignment optimization. Figure 4 shows the spectral response of our Ag_2Se / PbS /Ag_2Se QD barrier device measured at room temperature. A good agreement in the spectral shape of our device spectral responsivity data and the optical absorption of Ag_2Se QD (Figure 2(a)) indicates that photocurrent majorly arise from Ag_2Se QDs. Compared to the previous generation of QD barrier devices (8), mid-wavelength infrared responsivity across 3 – 5 μm was approximately enhanced by 6.3 times. This is mainly attributed to the minimization of transport barrier for photoexcited electrons. A peak responsivity occurs at 4.5 μm with a value of 84.1 mA/W and the corresponding external quantum efficiency (EQE) is 2.32 %. The noise current density of our device was also measured at room temperature. The measured value at 15 Hz with 1 Hz bandwidth was 10^{-9} $A \cdot Hz^{-1/2}$ and the resulting specific detectivity (D*) is 2×10^6 Jones. This is approximately 570 % improvement compared to QD barrier device without energy level alignment optimization.

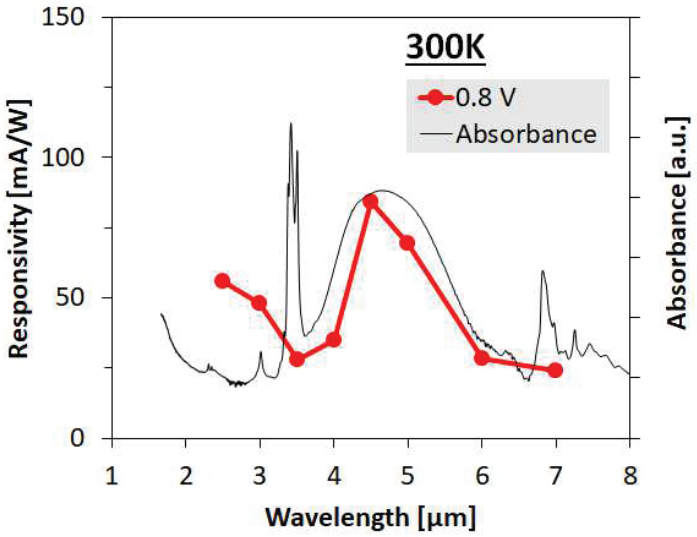

Figure 4. Spectral responsivity obtained from Ag_2Se / PbS /Ag_2Se QD barrier device. The measurements were conducted at room temperature 300 K with 0.8 V bias at 15 Hz. Optical absorbance spectra of Ag_2Se QD is overlaid for comparison.

Conclusion

In summary, we have fabricated vertically-stacked barrier device with optimized QD energy level alignment. The optimization leads to 910% increase in dark resistivity, accompanied by 532 % increase in the mid-wavelength infrared responsivity reaching 84.1 mA/W. Overall, 570% increase in specific detectivity is measured compared to un-optimized first generation barrier devices. Further improvements in the device performance are anticipated by having a complimentary n- and p-type barrier (12).

Acknowledgments

This work was supported by National Science Foundation Grant No. ECCS-1809112.

References

1. D. V. Talapin, J. S. Lee, M. Kovalenko and E. Shevchenko, *Chem. Rev.,* **110**, 389-458 (2010).
2. G. Konstantatos and E. H. Sargent, *Proc. IEEE*, **97**, 1666-1683 (2009).
3. T. Nishihara, H. Tahara, M. Okano, M. Ono and Y. Kanemitsu, *J. Phys. Chem. Lett*., **6**, 1327–1332 (2015).
4. C. Melnychuk and P. Guyot-Sionnest, *ACS Nano*, **13**, 10512- 10519 (2019).
5. J. Piotrowski, *Opto-Electron. Rev.*,**12**, 111–122 (2004).
6. M. Chen, X. Lan, X. Tang, Y. Wang, M. H. Hudson, D. V. Talapin and P. Guyot-Sionnest, *ACS Photonics*, **6**, 2358-2365 (2019).

7. S. Hafiz, M. R. Scimeca, P. Zhao, I. J. Paredes, A. Sahu and D. -K. Ko, *ACS Appl. Nano Mater.*, **2**, 1631-1636(2019).
8. S. B. Hafiz, M. M. A. Mahfuz and D.-K. Ko, *ACS Appl. Mater. Interfaces*, **13**, 937–943 (2021).
9. M. A. Hines and G. D. Scholes, *Adv. Mater.*, **15**, 1844-1849 (2013).
10. J. Jasieniak, M. Califano and S. E. Watkins, *ACS Nano*, **5**, 5888-5902 (2011)
11. J. Qu, N. Goubet, C. Livache, B. Martinez, D. Amelot, C. Gréboval, A. Chu, J. Ramade, H. Cruguel, S. Ithurria, M. G. Silly, and E. Lhuillier, *J. Phys. Chem. C*, **122**, 18161-18167 (2018).
12. P. Martyniuk, M. Kopytko and A. Rogalski, *Opto-Electron. Rev.*, **22**, 127-146 (2014).